Electroreduction of water, a promising alternative to gas injection: A case on hydrogen solubilization in biological processes involving hydrogenotrophs

Juan-Diego Carvajalino-Olave, Léa Laguillaumie, Claire Dumas, Benjamin Erable

Electroreduction of water, a promising alternative to gas injection: A case on hydrogen solubilization in biological processes involving hydrogenotrophs

Juan-Diego Carvajalino-Olave [a,b,*], Léa Laguillaumie [a], Claire Dumas [a], Benjamin Erable [b]

[a] TBI, University of Toulouse, INSA, INRAE, CNRS, Toulouse, France
[b] Laboratoire de Génie Chimique, Université de Toulouse, CNRS, INPT, UPS, Toulouse, France

ARTICLE INFO

Keywords:
Hydrogen supersaturation
Water electrolysis
Bubble nucleation
Solventogenesis
Microbial electrosynthesis

ABSTRACT

Hydrogenotrophic microorganisms reduce organic or inorganic molecules coupled with the oxidation of H_2, for the production of valuable products such as carboxylic acids, methane, and ethanol, as well as the reduction of sulfates, nitrates or iron for remediation applications. H_2 is usually dissolved by gas injection but the low gas-to-liquid mass transfer limits its biotic uptake. This study proposes water electroreduction (WE) as an alternative to gas injection (GI) for dissolving H_2. First, WE and GI were compared in terms of H_2 solubilization rate, efficiency, and maximum dissolved concentration in a 0.8 L potassium phosphate buffered medium (0.1 mol·L^{-1}, pH = 7.2) used as a representative medium for the enrichment and study of hydrogenotrophic microorganisms. Although the H_2 production rate of WE was around 18 times lower than the H_2 supply rate used during GI, both techniques achieved similar H_2 solubilization rate but different solubilization efficiencies. To reach a solubilization rate of 0.67 mmol·L^{-1}·h^{-1} by WE, 1.87 mmol·h^{-1} of H_2 were produced, yielding a 35 % solubilization efficiency. In contrast, achieving a comparable solubilization rate of 0.79 mmol·L^{-1}·h^{-1} via GI required an injection of 42 mmol·h^{-1}, corresponding to a solubilization efficiency of only 2 %. Moreover, the maximum concentration of dissolved H_2 reached (0.62 mmol·L^{-1}) by GI was limited by the saturation concentration at 1 bar (0.78 mmol·L^{-1}), while by WE it reached 1.21 mmol·L^{-1}. WE holds strong potential as a H_2 source for biological processes involving hydrogenotrophs where high H_2 concentrations are desirable to enhance metabolite production rates and selectivity.

1. Introduction

Hydrogenotropic microorganisms can reduce a wide variety of substrates such as carboxylic acids, aldehydes, alcohols and inorganic molecules by using dissolved H_2 as electron source. From the 73 different hydrogenotrophic reactions compiled by Thauer et al [1], their application ranges from the reduction of organic/inorganic carbon for metabolites production (e.g., acetogenesis, methanogenesis and solventogenesis) to the reduction of inorganic electron acceptors for remediation applications (e.g., denitrification, sulfate reduction, ferric iron reduction) [1–6].

Controlling the H_2 concentration is fundamental for selecting specific strains within bioreactors with a mixed consortium of microorganisms, due to their specific kinetics, thermodynamics and energetics. As noted by Muñoz et al, strains with highest H_2 thresholds (minimum H_2 concentration required for making the H_2 uptake thermodynamically feasible) such as *Clostridium* sp. (threshold range: 2000–15,000 nmol·L^{-1}) are usually enriched in consortia with high H_2 concentrations, while at *Sporomusa* sp. (threshold range: 40–100 nmol·L^{-1}) are enriched at low H_2 concentrations, in hand with methanogens [7]. As an example, working at low H_2 concentrations would help favoring the competition of methanogens [8,9].

Muñoz et al found that different species of hydrogenotrophic acetogens (*Clostridium* sp., *Sporomusa* sp. and *Acetobacterium* sp.) were not inhibited by high concentrations of H_2 up to saturation concentration, (just below 0.78 mmol·L^{-1} at 1 bar of H_2) and its H_2 consumption rate followed first-order kinetics [10]. Besides favoring the production rate of metabolites, additional reducing equivalents in the form of H_2 are

required to shift acetogenesis into solventogenesis to favor organic acids elongation. The longer the organic acids the better the added value. Stoichiometrically, 4 mol of H_2 are needed to reduce 2 mol of CO_2 into 1 mol of acetate (H_2:CO_2 = 2:1), but 2 additional H_2 moles are needed to reduce 1 mol of acetate into ethanol (H_2:CO_2 = 3:1).

In summary, the maintenance of high H_2 concentrations influences the competition among hydrogenotrophic species and the selection of other metabolites while also maintaining high H_2 uptake rates (not limited by the classical substrate saturation found in Monod-like growth kinetics). In practice, maintaining high concentrations of H_2 in the liquid medium is technically challenging. The limitations and their work-arounds are described in the following sections.

1.1. Limitations on achieving high H_2 concentration in the liquid medium with gas injection

The traditional approach to supply H_2 in bioreactors is to inject H_2 gas into the liquid. Around two thirds of the total H_2 production in 2023 came from steam methane reforming (SMR), with water electrolysis accounting for less than 1 % of the global production [11]. The main drawback of using gas injection is the slow gas-to-liquid mass transfer of H_2 due to the low solubility of H_2 in water [12] (45 times lower than CO_2 at 1 atm and 25C [webbook.nist.gov]). In processes where hydrogenotrophs are involved, H_2 becomes the limiting substrate since only the dissolved H_2 becomes bioavailable. Two different approaches have been found in literature so far to overcome this limitation: 1) Increasing the gas-to-liquid H_2 transfer by improving the reactor design or 2) bypassing the gas-to-liquid mass transfer by avoiding the use of gaseous H_2. These two approaches are depicted in Fig. 1.

1.1.1. First approach: improving the gas-to-liquid H_2 transfer

In practical applications where gas is injected through coarse/fine gas spargers, the resulting injected bubbles usually have diameters in the millimeter range. The solubilization rate of these millimetric bubbles is widely described by Eq. (1):

$$\frac{dC_{H2}}{dt} = K_L a\left(C_{H_2}^{*} - C_{H2}(t)\right) \quad (1)$$

Here, $\frac{dC_{H2}}{dt}$ is the rate of H_2 solubilization, K_L is the overall liquid mass transfer coefficient, a is the gas-liquid interfacial area, $C_{H2}(t)$ is the dissolved H_2 concentration and $C_{H_2}^{*}$ is the dissolved H_2 concentration at saturation. Increasing either K_L, a or $C_{H_2}^{*}$ results in an increased solubilization rate. k_L can be increased by the energy inputs such as agitation in the medium and the increase of bubble residence time such as in tall bubble columns [13,14]. On the other hand, producing a large number of bubbles of small diameter is desired to increase the interfacial surface area, which can be achieved using gas spargers with small orifices. Unfortunately, spargers with small orifices are prone to get clogged by biomass, particulate organic matter and salt precipitates from the liquid medium, which may require often maintenance. Additionally, if orifices are too close to each other, bubbles may coalesce more easily (increasing bubble size) before departing the sparger surface [14]. Other approaches less stablished such as hollow membranes, trickle-bed reactors and small bubble injection also aim to increase the interfacial area and are already being used in bioprocessing studies [15,16]. Lastly, higher $C_{H_2}^{*}$ values can be obtained by increasing the gas pressure in contact with the liquid

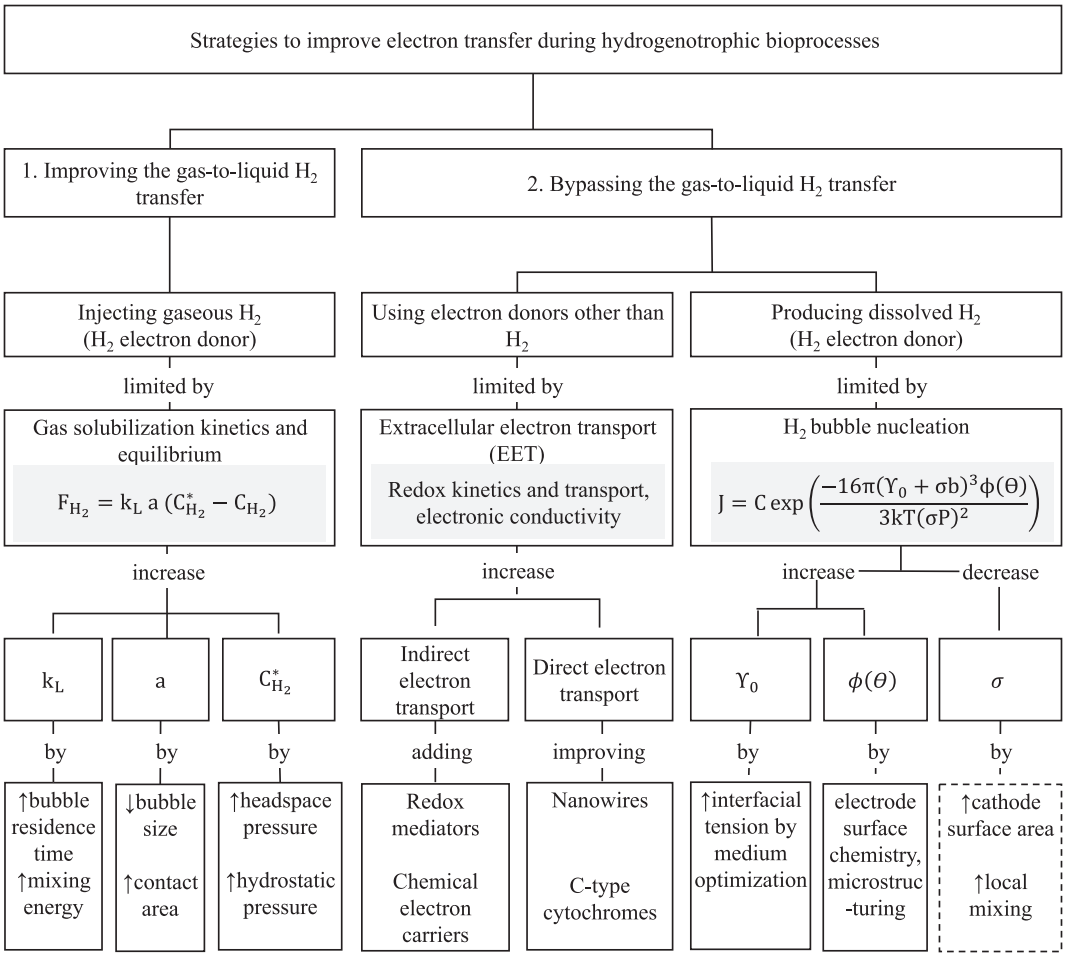

Fig. 1. Scheme of strategies to be used to improve electron transfer during gas fermentation. The approach delimited by a dashed line is proposed here in this article.

as shown in Eq. (2) representing Henry's law.

$$C_{H_2}^{*} = k_H(T)\, P_{H_2} \quad (2)$$

where k_H is Henry's law constant and P_{H_2} is the partial pressure of H_2. For example, 0.78 mmol·L^{-1} of dissolved H_2 is at equilibrium with 1 bar of H_2 in the gas phase at 25C [17]. Although this can be achieved either using tall columns with higher hydrostatic pressure, increasing the headspace pressure in pressurized reactors is also done for this purpose with the disadvantage of the operational and safety complexities that brings the working with pressurized reactors.

Another approach to increase the saturation concentration would be the injection of fine/ultrafine bubbles that should solubilize due to high internal pressures [18]. Nevertheless, working with nano/micrometric size bubbles is not common in the industry yet.

1.1.2. *Second approach: bypassing the gas-to-liquid H_2 transfer*

In the second approach, the gas-to-liquid mass transfer limitation is bypassed by replacing H_2 gas injection with: A) electron sources other than H_2 and B) electrochemical production of dissolved H_2.

1.1.2.1. Using electron sources other than H_2 for biological transformation. Some microorganisms can perform extracellular electron transport (EET) with conductive solid surfaces and molecules outside the cell membrane such as electrodes and redox mediators. These "electroactive" bacteria can either perform a direct or indirect EET. In direct electron transport, a biofilm forms on the electrode surface where the relay of electrons occurs through conductive "nanowires" or by membrane-bound cytochromes [19]. In indirect electron transport, redox mediators such as methyl viologen (externally added) and flavins (produced biologically in-situ) get continuously oxidized/reduced between the electrode and the microorganisms [20]. Other molecules such as formate, ammonia and Fe^{2+} can be electrochemically produced and used as soluble electron carriers during the fermentation of gases, but reported product yields from Fe^{2+}/NH_3 oxidizers have been comparatively lower than using H_2 by hydrogenotrophic acetogens/methanogens [21,22].

When electrodes (cathodes) work as electron donors for electroactive bacteria, the bioprocess is commonly called microbial electrosynthesis (MES) [23]. Similarly to common hydrogenotrophic bacteria, acetate, methane and alcohols are also the main products usually targeted [24]. While some hydrogenotrophic acetogens have been reported to be able to perform EET in electroactive biofilms attached to the electrode, the reduced spatial distribution of cells in contact with the electrode surface might limit the electron transfer [25].

1.1.2.2. Production of dissolved H_2 by water electroreduction. The production of hydrogen by water electroreduction presents advantages regarding the production using fossil fuels such as reforming. However, several challenges need to be faced. Indeed, the parameters that are influencing the electroreduction of water are the current density applied (consumed). The furnished energy is depending on the internal resistance of the system that is influenced by the membrane, the electrolytes, the electrodes materials and shapes…. In this study all the parameters of the reactors are constant, only the applied current will be studied.

The produced H_2 in a cathodic surface by water electroreduction does not immediately evolves into the gas phase. H_2 molecules are first produced and dissolved in the liquid phase. The first requisite for the bubble evolution is to surpass a certain concentration threshold, which is larger than the saturation concentration (therefore, bubble nucleation occurs at a local supersaturation of H_2). The rate of bubble nucleation can vary according to cathode irregularities and its surface chemistry, and the interfacial tension between the gas-liquid phase [26] as shown in Eq. (3):

$$J = C \exp\left(\frac{-\Delta G(C_{H_2})}{kT}\right)$$

$$\Delta G(C_{H_2}) = \frac{16\pi(\Upsilon_0 + \sigma b)^3 \phi(\Theta)}{3(\sigma P)^2} \quad (3)$$

where J is the bubbling rate, C is a pre-exponential factor and $\Delta G(C_{H_2})$ is an exponential factor that depends on the surface tension of the liquid (Υ_0), the supersaturation ratio ($\sigma = \frac{CH_2}{CH_2^{crit}} - 1$) and $\phi(\Theta)$ which is a function that goes from 1 to 0 as the contact angle of the bubble in the nucleation site increases. The nucleation of bubbles reduces the solubilization efficiency which is undesirable for hydrogenotrophic processes. To reduce the bubbling rate J, it would be possible to increase the interfacial tension, the wettability, or reduce the local supersaturation near the cathodic surface.

Increasing the surface tension of a liquid might be harder to achieve than reducing it using surfactants. Surfactants tend adsorb at the cathode surface which in turn reduce the current necessary to start the nucleation of bubbles [27,28]. Wettability has also been studied in abiotic electrolyzers with the goal of fast H_2 gas formation and removal. For example, the increase of bubble coalescence and formation of large bubbles was favored when the surface of a nickel foam cathode was coated with PTFE due to the decrease in wettability [29]. The local concentration of dissolved H_2 can be decreased in reactors when the current density is homogeneously distributed on the cathode surface. This can be achieved by using porous electrodes with large surface area per occupied volume. Also, efficient mixing of the catholyte should reduce the local accumulation of H_2 near the cathode surface. In a MES, the oxidation of electrochemically produced H_2 and the reduction of CO_2 by *M. maripaludis*, using 3D-printed electrodes with large surface area per volume allowed to reduce the H_2 waste due to the absence of bubble nucleation [30].

It has been suggested that a MES for CO_2 reduction with mixed cultures may work preferably with indirect EET, where H_2 is produced at the electrode surface and once dissolved, quickly consumed by the surrounding hydrogenotrophs [31,32]. The slow kinetics of biofilm electron uptake vs H_2-mediated electron uptake are also discussed elsewhere in favor of using planktonic bacteria for CO_2 reduction in a MES [16].

1.2. *Novelty of this work*

The majority of previous investigations have focused on supplying H_2 to hydrogenotrophic microorganisms via conventional gas sparging or through the electrochemical generation of bubbles during water reduction. By contrast, the present study specifically examines the electrochemical production of dissolved H_2 as the primary electron donor, thereby circumventing the mass transfer limitations inherent to bubble-mediated delivery.

While the advantages of dissolved H_2 over gaseous H_2 supply for hydrogenotrophic processes have been proposed in the past [30], to the best of our knowledge, this work represents the first systematic comparison between water electroreduction and gas sparging with respect to (i) achievable H_2 solubility, (ii) solubilization kinetics, (iii) process efficiency, and (iv) energy requirements. In addition to quantifying these performance metrics, this study introduces a novel modeling framework that integrates the distinct solubilization kinetics of both methods with the biological uptake kinetics for hydrogenotrophic competition and product selectivity. Our thermodynamic analysis reveals new opportunities for coupling electrochemical H_2 delivery with bioprocess design and optimization.

It is important to emphasize that, unlike studies exploring multiple operational variables (e.g., temperature, pH, electrolyte composition, electrode materials, or hydrodynamics [33–36]), the present work

evaluates the effect of current density, which is a key controllable parameter in electrochemical H_2 production, and directly compares it with different gas injection rates. This approach enables a clear, quantitative assessment of the potential of water electroreduction for sustaining hydrogenotrophic activity under controlled conditions. Collectively, these findings constitute an important step towards demonstrating the practical value of electrochemically generated dissolved H_2, highlighting its potential for future application in fermentation systems.

2. Materials and methods

2.1. Reactor setup used for both H_2 solubilization techniques

A potassium phosphate buffer solution was used as liquid medium (electrolyte) containing 10.7 $g{\cdot}L^{-1}$ of K_2HPO_4 and 5.2 $g{\cdot}L^{-1}$ of KH_2PO_4 (pH = 7.2) to simulate the buffering capacity of a growth medium used for acetogenesis in a microbial electrosynthesis cell [37]. The liquid medium was sparged with N_2 gas for 10 min using a glass frit (VitraPOR Micro-immersion-filter Por 2, Robu, Germany) of 10 mm of diameter and 4 mm of thickness, prior to the start of each experiment to remove traces of dissolved gases such as H_2 and O_2. A two-chamber H-type cell (Duran Schott GLS 80® with side connection) was used as a reactor with a 4-port screw cap (Duran GLS 80 ® 4-port EPDM seal), with a working volume of 800 mL on each chamber and separated by a cation exchange membrane of 5 cm of diameter (CMI 7000S, Membranes International Inc., USA) as shown in Fig. 2A. The liquid medium was agitated with a magnetic stirrer at 370 rpm in both H_2 solubilization techniques. The dissolved H_2 concentration was measured using an electrochemical H_2 probe (MS08, Aquams, France). The H-type cell was open to air through one of the screw cap ports to avoid the impact of different headspace pressures on the solubilization of H_2. Therefore, a small ingress of oxygen to the liquid could be expected (and get reduced in the catholyte) but its concentration does not interfere with the H_2 sensor readings (although a diminished solubilization efficiency during water electroreduction could be expected). At the end of each experiment, the dissolved H_2 concentration of a liquid sample of 50 mL was measured by equilibrating the aliquot with a 5 mL headspace and further analyzed with the headspace gas chromatography method (See Supplemental Information for further details).

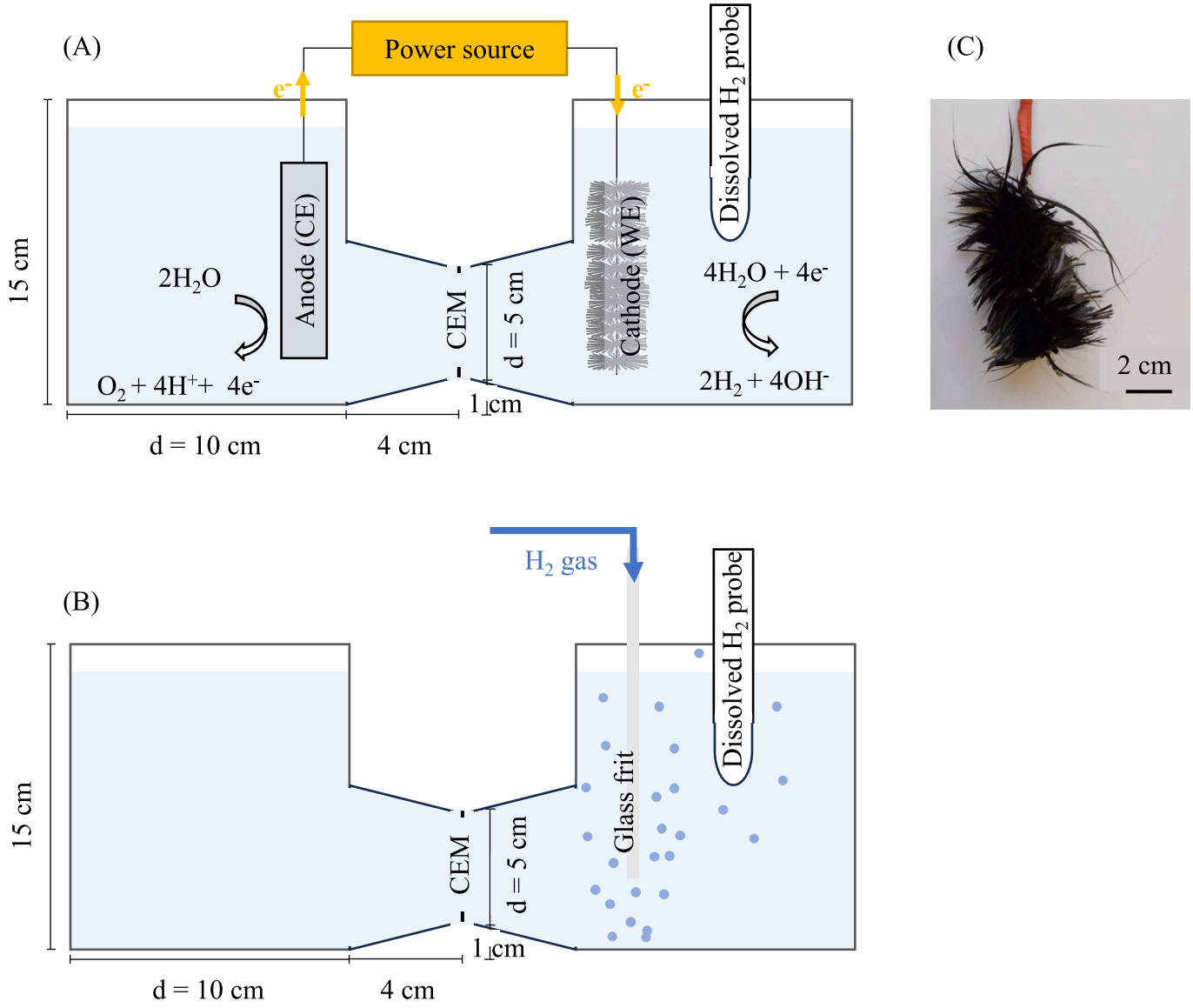

Fig. 2. Experimental setup of the two-chamber H-type cell used during (A) water electroreduction and (B) H_2 gas injection. The cathode material used during water electroreduction is shown in (C). CE: Counter electrode (DSA anode); WE: Working electrode (Carbon brush cathode); CEM: Cation exchange membrane.

For the water electroreduction technique, a DSA® plate of 2.5 × 5.3 × 0.1 cm (projected area: 13.25 cm^2; Di Noer Technology Co. Ltd., China) was used as a counter electrode (i.e., anode here). A carbon brush (6TMIC Ing. France) occupying a diameter of 5 cm and 8 cm of height (projected surface area: 40 cm^2, bulk volume: 157 cm^3) was used as a working electrode (i.e., cathode here, Fig. 2C). Prior to its use, the carbon brush was thermochemically treated by thermal activation in a muffle furnace at 380C for 2 h. Afterwards, the carbon brush was cleaned by successively immersion in the following solutions under stirring: Ethanol:Acetone (1:1) for 20 min, distilled water for 20 min, 1 M HCl for 1 h, distilled water for 20 min, 1 M NaOH for 1 h, and distilled water for 20 min. A titanium and stainless-steel rod were used as current collectors respectively for the working and counter electrodes.

For the H_2 gas injection technique, no electrodes were submerged in any compartment. Instead, a glass frit (VitraPOR Micro-immersion-filter Por 2, Thermo Fisher Scientific, France) was used for the H_2 gas injection as shown in Fig. 2B.

2.2. Design of experiments

Three different H_2 supply rates were used for each one of the H_2 solubilization techniques evaluated. The values of each H_2 supply rate and their corresponding fixed current and gas injection rates are summarized in Table 1.

The lowest current applied, 20 mA, was chosen due to allowing to reach a steady state concentration in around 5 h (smaller currents could take longer, making the experiment unnecessarily long), while 100 was the maximum current it could be imposed before reaching the cell voltage security limits (10 V) in the H-type cell. For H_2 gas injection, a mass flow meter (Bronkhorst EL-FLOW select, France) was used to set the H_2 supply rate between 1 L·h-1 (minimum to overcome the glass frit pressure drop) and 3 L·h-1 (maximum allowed by the flow meter).

A potentiostat (VSP, BioLogic) was used as a power source to perform chronopotentiometry (CP) for applying a constant current at the working electrode during the production of dissolved H_2 through water electroreduction. For H_2 gas injection, a mass flow meter (Bronkhorst EL-FLOW select, France) was used to set the H_2 supply rate.

2.3. Solubilization rate and efficiency

The solubilization rate [$mmol{\cdot}L^{-1}{\cdot}h^{-1}$] was calculated by dividing the concentration change by the time it takes to increase the concentration of dissolved H_2 from 0 to 0.5 $mmol{\cdot}L^{-1}$ per liter of liquid medium. Values larger than 0.5 $mmol{\cdot}L^{-1}$ were not used for the calculation since the H_2 solubilization rate with gas injection quickly drops at larger values due to approaching the saturation concentration.

The percentual solubilization efficiency (η) was calculated for every point in time as shown in Eq. (4):

$$\eta(t) = 100{\cdot}\frac{n_d(t)}{n_s(t)} \tag{4}$$

$$n_d(t) = \frac{V_c{\cdot}C_{H_2}(t)}{MW}$$

Table 1
Experimental conditions evaluated for each H_2 solubilization technique.

H_2 solubilization technique	H_2 supply rate [$mmol{\cdot}h^{-1}$]
Water electroreduction	
20 mA	0.37
60 mA	1.12
100 mA	1.87
H_2 gas injection	
1 $L{\cdot}h^{-1}$	42
2 $L{\cdot}h^{-1}$	83
3 $L{\cdot}h^{-1}$	125

$$n_s(t) = \frac{Q_{H_2}{\cdot}t}{V_M} \tag{4}$$

where n_d are the moles of H_2 dissolved in the liquid [mmol]; n_s are moles of H_2 supplied in the system (by gas injection or water electroreduction) [mmol]; V_c is the volume of the catholyte (0.8 L); $C_{H_2}$is the measured dissolved H_2 concentration [$mg{\cdot}L^{-1}$]; MW is the molar weight of H_2 [2 $mg{\cdot}mmol^{-1}$], Q_{H_2} is the volumetric H_2 supply rate [$nL{\cdot}h^{-1}$]; t is the time of measurement [h]; and V_M is the molar volume [0.024 L ·$mmol^{-1}$ at 1 bar and 20 °C].

For the H_2 solubilization kinetics comparison between the biological uptake rate and the solubilization rate, the datapoints from dissolved H_2 concentration vs time were first smoothed through a median filter (*medfilt1* MATLAB's function). The solubilization rate was then calculated using the gradient of the concentration over time (*gradient* MATLAB's function) and finally, a linear model was fitted between the solubilization rate and the dissolved H_2 concentration (*fitlm* MATLAB's function).

2.4. Energy consumption

The energy consumption was calculated using the solubilization rate measured between 0 and 0.5 $mmol{\cdot}L^{-1}$ as described above. The energy consumption is expressed as MJ per mol of solubilized H_2. For water electroreduction, the energy consumed per mol of solubilized H_2 (E_{we}) is calculated as shown in Eq. (5):

$$E_{we} = (V_{cell}{\cdot}I)\frac{1}{Vol{\cdot}R_{sol}}{\cdot}\left(\frac{1\ MJ}{1x10^6\ J}\right) \tag{5}$$

where V_{cell} [V] is the cell voltage, I [A] is the imposed current, Vol [8 × 10^{-4} m^3] is the liquid medium volume, and R_{sol} [$mol{\cdot}m^{-3}{\cdot}s^{-1}$] is the H_2 solubilization rate. For the calculation of the energy consumption, the first approximation was to include the energy consumed during the production of H_2 with the energy consumed during the compression. The energy consumed during the production per mol of H_2 solubilized (E_{smr}) was calculated based on a life cycle analysis done on the steam methane reforming process, using the total energy used by the system (natural gas and non-feedstock): 183.2 MJ/kg H_2 [38] and using it in Eq. (6):

$$E_{smr} = 183.2\frac{MJ}{kg\ H_2}{\cdot}\left(\frac{0.002\ kg\ H_2}{1\ mol\ H_2}\right){\cdot}\frac{R_{sup}}{Vol{\cdot}R_{sol}} \tag{6}$$

where R_{sup} [$mol{\cdot}s^{-1}$] is the H_2 supply rate. To calculate the compression energy, it was calculated first the required pressure to overcome the pressure drop from the glass frit (ΔP_{frit} [Pa]) using Darcy's law in Eq. (7):

$$\mathbf{\Delta P_{frit}} = \frac{\mathbf{R^V_{sup}{\cdot}\mu_g{\cdot}L}}{\mathbf{k{\cdot}A}} \tag{7}$$

where R^V_{sup} is [$m^3{\cdot}s^{-1}$] the H_2 supply rate in volumetric units, μ_g[8.9 × 10^{-6} Pa·s] is the dynamic viscosity of H_2, L [0.004 m] is the glass frit thickness, k [2.9 × 10^{-11} m^2] is Darcy's permeability of the glass frit, and A [7.85 × 10^{-5} m^2] is the cross-sectional area of the glass frit. The energy of compression per mol of H_2 solubilized (E_{comp}) can be calculated using Eq. (8):

$$E_{comp} = \left(\frac{R_{sup}}{Vol{\cdot}R_{sol}}\right){\cdot}\left(\frac{1}{\in}{\cdot}R{\cdot}T{\cdot}\ln\left(\frac{P_2}{P_1}\right)\right){\cdot}\left(\frac{1\ MJ}{1x10^6\ J}\right) \tag{8}$$

where ∈ [0.8 unitless] is the energy efficiency of compression, R [8.314 $J{\cdot}mol^{-1}{\cdot}K^{-1}$] is the ideal gas constant, T [298.15 K] is the temperature, P_2 [Pa] is the pressure needed to overcome the pressure drop from the glass frit and P_1 [Pa] is the inlet pressure to the compressor coming from the steam methane reforming process. A quick calculation ΔP_{frit} for the case where H_2 is supplied at a rate of 125 $mmol{\cdot}h^{-1}$ [R^V_{sup} = 8.3 × 10^{-7}

$m^3 \cdot s^{-1}$] would result in a very small $\Delta P_{frit} = 13$ Pa. Even assuming a large compression work from 1 bar to 250 bar (high pressure H_2 gas cylinder), this would result in the energy of compression being around 5 % of the energy used during the H_2 production by steam methane reforming. Therefore, the calculations for energy consumption in gas injection only consider the energy associated with the H_2 production by steam methane reforming.

A third hypothetical case was evaluated where H_2 was produced with an ideal water electrolyzer at 1.48 V [39] producing H_2 gas with a solubilization efficiency of $e_{sol} = 1.5\%$ (based on the experimental results obtained here for gas injection). Assuming all of the electric current imposed is converted to H_2 gas, we can express $R_{sol} = e_{sol} \cdot I$ and calculate the energy consumption by using Eq. (5).

2.5. Modeling the thermodynamic potential of hydrogenotrophic reactions at different H_2 solubilization kinetics

A comparison of the thermodynamic potential (feasibility) of different hydrogenotrophic reactions as a function of the H_2 concentration is done based on their Gibbs free energy change as shown in Table 2. To establish the feasibility at operational conditions during hydrogenotrophic processes, the following mass balance on the H_2 and CO_2 concentration was solved at steady state $\left(\frac{dC_i}{dt} = 0\right)$ to simulate a continuous bioreactor where H_2 and CO_2 are consumed by hydrogenotrophic acetogens as shown in Eqs. (9) and (10):

$$\frac{dC_{H_2}}{dt} = -k_1^x X(C_{H_2}) + K_L^{H_2} a\left(C_{H_2}^{sat} - C_{H_2}\right) \quad (9)$$

$$\frac{dC_{CO_2}}{dt} = -\frac{k_1^x X}{Y}(C_{H_2}) + K_L^{CO_2} a\left(C_{CO_2}^{sat} - C_{CO_2}\right) \quad (10)$$

where k_1^x is the biomass specific H_2 uptake rate, X is the biomass concentration, $C_{H_2}^{sat}$ and $C_{CO_2}^{sat}$ are the gas saturation concentrations characteristic of the solubilization technique, Y is the stoichiometric ratio of CO_2 to H_2 uptake and $K_L^{H_2}a$ and $K_L^{CO_2}a$ are the overall mass transfer/solubilization coefficients. The values taken for these parameters were chosen to represent the two scenarios under different H_2 solubilization limitations, and their values are tabulated in Table 3.

In the first scenario, it is assumed that the process is limited by the H_2 solubilization rate, characterized by low $K_L^{H_2}a$ to $k_1^x X$ ratios, while the second scenario assumes that there is no limitation by H_2 solubilization, characterized by larger $K_L^{H_2}a$ to $k_1^x X$ ratios, with the purpose of shifting acetate production to ethanol. For both scenarios, Y was taken as 2 (see stoichiometry of acetogenesis at Table 3) and $\frac{k_L^{CO_2}a}{k_L^{H_2}a}\sqrt{\frac{D_{CO_2}}{D_{H_2}}} = 0.65$ [40] were used for a system at steady state at 1 bar and 298 K. $C_{H_2}^{sat}$ was varied from 0.78 mmol·L^{-1} (characteristic of gas injection at 1 bar) to 5.5 mmol·L^{-1}, the latter corresponding to the supersaturation concentration experimentally found in microelectrode described by Lubetkin during water electroreduction [41].

Once the steady state concentrations of H_2 and CO_2 are obtained from the different kinetic scenarios described above, the ΔG_r of Acetogenesis and Ethanol production is calculated using Eq. (11):

$$\Delta G_r = \Delta G_r^{0'} + RT\ln(Q_r);$$

$$Q_r = \prod_j \left(a_j^{v_j}\right) \quad (11)$$

where R is the universal gas constant, T is the absolute temperature, a_j is the concentration of each specie and v_j is the stoichiometric coefficient of each specie, with reactants having a negative value. All calculations and simulation scenarios were performed in MATLAB R2024a (MathWorks Inc., Natick, Massachusetts, United States, RRID:SCR_001622).

Table 2
Standard Gibbs Free Energy of Reaction ($\Delta G_r^{0'}$) of different hydrogenotrophic reactions adjusted at pH = 7.

Reaction	Stoichiometry	$\Delta G_r^{0'}$ [kJ/reaction][1]
Sulfate reduction	$SO_4^{2-} + 4H_2 + H^+ \rightarrow HS^- + 4H_2O$	−94.8
Methanogenesis	$CO_2 + 4H_2 \rightarrow CH_4 + 2H_2O$	−131
Acetogenesis	$2CO_2 + 4H_2 \rightarrow CH_3COO^- + H^+ + 2H_2O$	−152
Ethanol production	$CH_3COO^- + H^+ + 2H_2 \rightarrow CH_3CH_2OH + H_2O$	−9.51

[1] The values of $\Delta G_r^{0'}$ were calculated by adjusting to pH = 7, the ΔG_r^0 obtained from the energies of formation compiled in the NBS tables [68].

3. Results

3.1. H_2 solubilization kinetics

The kinetics of H_2 solubilization obtained for each one of the techniques listed in Table 1 are shown in Fig. 3. At first sight, although the gas injection curves reached their saturation concentration faster than with water electroreduction, the maximum concentration of dissolved H_2 achieved was lower than the maximum concentration obtained during water electroreduction. For the three H_2 supply rates used for gas injection, the maximum dissolved H_2 concentration achieved varied from 0.58 mmol·L^{-1} to 0.62 mmol·L^{-1}, which was just below the theoretical equilibrium concentration of 0.78 mmol·L^{-1}. On the contrary, the maximum concentration of dissolved H_2 greatly varied with the H_2 supply rate during water electroreduction, from 0.51 to 1.21 mmol·L^{-1}, surpassing the equilibrium concentration of 0.78 mmol·L^{-1}. These supersaturation concentrations fall into the range previously reported by Kikuchi et al., where dissolved H_2 concentrations of 0.9–1.25 mmol·L^{-1} were obtained at the outlet of water electroreduction cells operated with a continuous fresh electrolyte flow [42,43]. They reported that the maximum concentration of dissolved H_2 achieved was limited at high current densities due to the accumulation of a high bubble population density and high bubble growth rate, which quickly transported the dissolved H_2 into the gas bubbles.

3.2. Variation of the maximum concentration of dissolved H_2 and solubilization rate with H_2 supply rate

The large variation of the maximum concentration of dissolved H_2 as a function of the H_2 supply rate can be better observed in Fig. 4A.

The fact that higher H_2 supply rates during water electroreduction lead to proportionally higher maximum dissolved H_2 concentrations opens up a new avenue for H_2 solubilization. Unlike gas injection, water electroreduction is not constrained by the H_2 saturation concentration achieved by the dissolution of H_2 bubbles, which could be advantageous for processes where besides having high H_2 solubilization rates, supersaturated concentrations of H_2 are also favorable. Although a higher concentration of dissolved H_2 was achieved during water electroreduction, the time it took to solubilize the same quantity of H_2 was faster for gas injection. This can be better observed by comparing the different solubilization rates as shown in Fig. 4B. Despite the ~2 orders of magnitude difference in H_2 supply rates, the H_2 solubilization rates obtained during water electroreduction were closely below those obtained during gas injection. For example, during water electroreduction at 1.87 mmol·h^{-1}, the H_2 solubilization rate obtained was 0.67 mmol·L^{-1}·h^{-1}, while during gas injection at 42 mmol·h^{-1} it was 0.79 mmol·L^{-1}·h^{-1}.

It is important to notice that even with the large difference in H_2 supply rates used in both techniques (around 20 times) the solubilization rates obtained were not largely different. It is expected therefore to have

Table 3
Kinetic parameters used for the study of the two kinetic scenarios simulated.

Scenario	$k_L^{H_2}a$ [h^{-1}]	k_1^x [$h^{-1}\cdot(g_{dw}\cdot L^{-1})^{-1}$]	X [$g_{dw}\cdot L^{-1}$] at steady state	$k_L^{H_2}a$ to k_1^xX ratio	
				Calculated	Range used
(1) Slow H_2 solubilization	0.062 [69]	60.93 [10]	1.4 [70]	7.27×10^{-4}	1×10^{-4} to 1×10^{-1}
(2) Fast H_2 solubilization	2280 [40]	8.19 [10]	0.5 [70]	557	1×10^{0} to 1×10^{3}

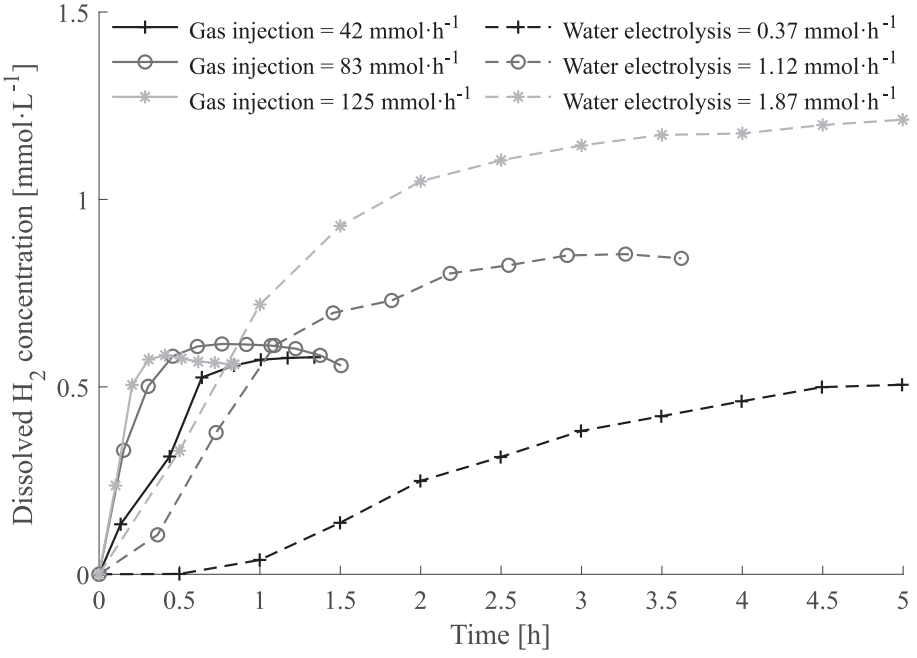

Fig. 3. H_2 solubilization kinetics by gas injection and water electroreduction in a potassium phosphate buffered solution (0.1 M, pH = 7.2) of 0.8 L. Three different H_2 supply rates were used in each case: For gas injection, 1 $L\cdot h^{-1}$ (42 $mmol\cdot h^{-1}$), 2 $L\cdot h^{-1}$ (83 $mmol\cdot h^{-1}$), and 3 $L\cdot h^{-1}$ (125 $mmol\cdot h^{-1}$); for water electroreduction, 20 mA (0.37 $mmol\cdot h^{-1}$), 60 mA (1.12 $mmol\cdot h^{-1}$), and 100 mA (1.87 $mmol\cdot h^{-1}$).

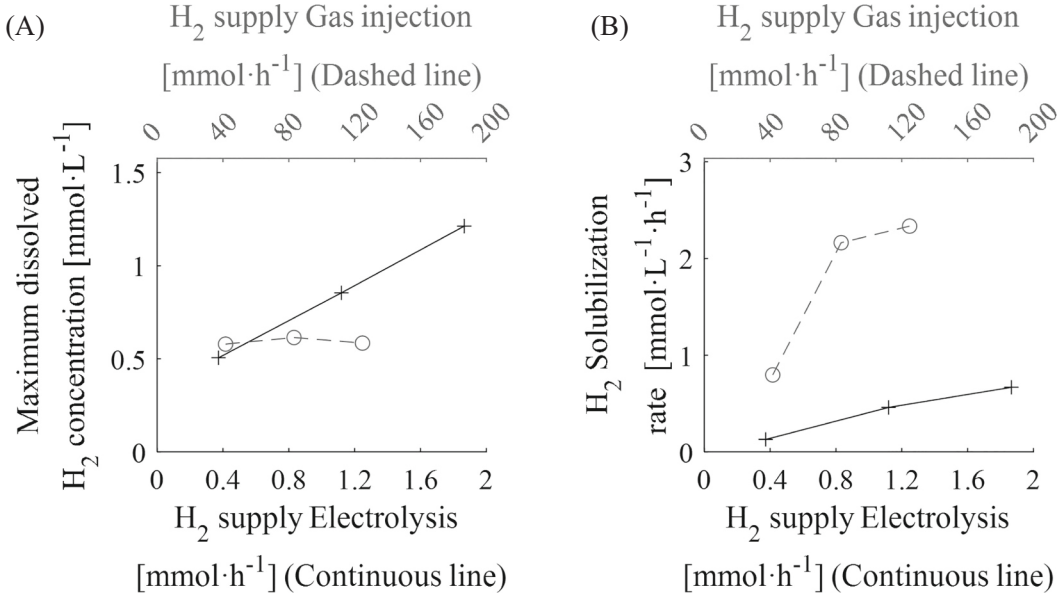

Fig. 4. Variation of the (A) maximum dissolved H_2 concentration and (B) H_2 solubilization rate as a function of the H_2 supply rate by water electroreduction and gas injection. The solubilization rate was measured from the time required to increase the concentration from 0 to 0.5 $mmol\cdot L^{-1}$.

largely different H_2 solubilization efficiencies between gas injection and water electroreduction. The different solubilization efficiencies achieved can be seen in Fig. 5. Overall, the H_2 solubilization efficiency by gas injection was ~2 %, much lower than the ~35 % reached by water electroreduction. The maximum solubilization efficiency achieved by water electroreduction at 1.12 $mmol\cdot h^{-1}$ was 41 % after 1 h of

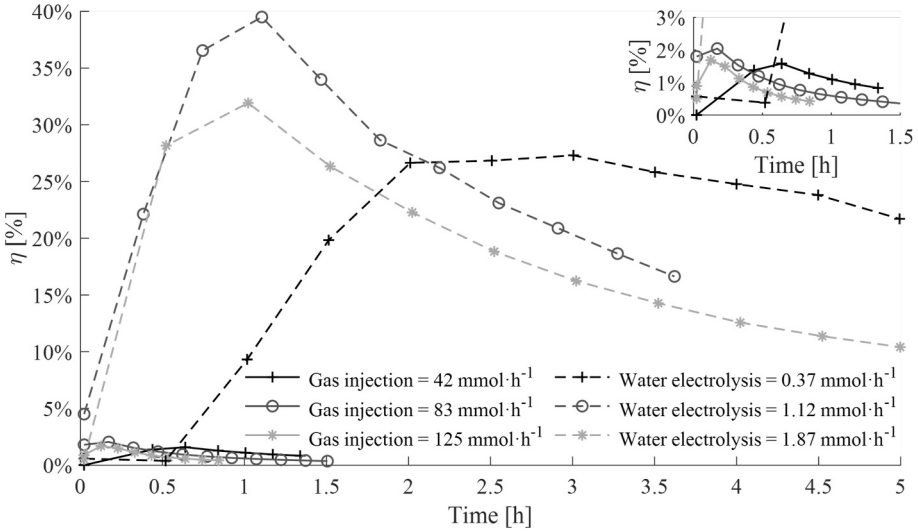

Fig. 5. Solubilization efficiency of dissolved H_2 by gas injection and water electroreduction in a potassium phosphate buffered solution (0.1 M, pH = 7.2) of 0.8 L. Three different H_2 supply rates were used in each case: For gas injection, 1 $L{\cdot}h^{-1}$ (42 $mmol{\cdot}h^{-1}$), 2 $L{\cdot}h^{-1}$ (83 $mmol{\cdot}h^{-1}$), and 3 $L{\cdot}h^{-1}$ (125 $mmol{\cdot}h^{-1}$); for water electroreduction, 20 mA (0.37 $mmol{\cdot}h^{-1}$), 60 mA (1.12 $mmol{\cdot}h^{-1}$), and 100 mA (1.87 $mmol{\cdot}h^{-1}$).

operation, which was around 20 times larger than the maximum achieved by gas injection, around 2 % after 10 min with a H_2 supply of 83 $mmol{\cdot}h^{-1}$. When comparing both techniques at similar solubilization rates, i.e., water electroreduction at 1.87 $mmol{\cdot}h^{-1}$ and gas injection at 42 $mmol{\cdot}h^{-1}$, the solubilization efficiency difference is of 18-fold.

Nevertheless, the release of H_2 bubbles was also observed after some time in the cathodic surfaces of the water electroreduction technique. For example, after 22 min at 1.87 $mmol{\cdot}h^{-1}$, H_2 bubbles started to slowly nucleate at the outer region of the carbon brush. Afterwards, the rate of bubble nucleation kept increasing until most of the cathode surface of the carbon brush became covered by bubbles by the end of the experiment (300 min). Using larger currents implies also using electrodes with larger surface areas so the local current at the electrode surface remains low enough to avoid fast nucleation and maintain or even upgrade high solubilization efficiencies.

3.3. *Energy consumed per mol of H_2 solubilized*

It is now useful to compare how the 18-fold difference in solubilization efficiency translates into energy efficiency. It is commonly accepted that electrolyzer are more energetically demanding for producing H_2 than the traditional steam methane reforming when considering the production of gaseous H_2. As hydrogenotrophic reactions require dissolved H_2, the energy consumption of each technique is normalized per each mol of H_2 solubilized and shown in Table 4.

At a H_2 supply rate of 42 $mmol{\cdot}h^{-1}$ by gas injection and 1.87 $mmol{\cdot}h^{-1}$ by water electroreduction, the energy required for solubilizing 1 mol of H_2 by water electroreduction was around 4.6-times lower than the energy required by gas injection if the H_2 gas was produced by SMR 3.6-times lower if it was produced by an ideal water electroreduction cell operating. This highlights the potential of water electroreduction as an efficient technique for the production of dissolved H_2.

Table 4
Estimation of the energy consumption per mol of H_2 solubilized for the gas injection and water electroreduction techniques evaluated at the conditions of this work.

H_2 solubilization technique	H_2 supply rate [$mmol{\cdot}h^{-1}$]	Solubilization rate [a] [$mmol{\cdot}L^{-1}{\cdot}h^{-1}$]	Energy per mol of H_2 solubilized [$MJ{\cdot}mol^{-1}$]
Gas injection	42	0.79	23.92 [b]
Gas injection	83	2.16	17.60 [b]
Gas injection	125	2.33	24.47 [b]
Water electroreduction	0.37	0.13	2.04[c]
Water electroreduction	1.12	0.46	3.20[c]
Water electroreduction	1.87	0.67	5.16[c]
Ideal water electroreduction with H_2 gas production	35[d]	0.67[d]	18.65[e]

[a] Calculated from the concentration change at 0 and 0.5 $mmol{\cdot}L^{-1}$ of dissolved H_2 in the 0.8 L liquid medium.
[b] Calculated from the production of H_2 by steam methane reforming, using the total energy used by the system (natural gas and non-feedstock): 183.2 MJ per kg H_2 [38].
[c] Calculated with the cell voltage at 0.5 $mmol{\cdot}L^{-1}$ of dissolved H_2 which corresponded to 2.92, 5.45 and 7.66 for the H_2 supply rates [$mmol{\cdot}h^{-1}$] of 0.37, 1.12 and 1.87.
[d] The solubilization rate was assumed to be the same as for water electroreduction at the highest supply rate, but the supply rate was calculated based on a 1.5 % solubilization efficiency (obtained in this work for gas injection).
[e] Calculated with a water electroreduction cell voltage of 1.48 V [39].

3.4. *Modeling of the effect of H_2 solubilization kinetics on hydrogenotrophic reactions*

For each H_2 solubilization technique, the highest rate of H_2 solubilization rate is obtained when the liquid medium is initially free of dissolved H_2. This solubilization rate then gradually decreases, eventually reaching zero, as the concentration of dissolved H_2 approaches the maximum amount that each system can hold. As the solubilization rate becomes a unique function of the dissolved H_2 according to the solubilization technique used, it becomes necessary to contrast the H_2 solubilization kinetics of each technique with the expected H_2 uptake kinetics for some hydrogenotrophic reactions to obtain information about the dissolved H_2 concentration that could be maintained at each case. In a continuous bioreactor working with a single strain where H_2 is being solubilized along with its biotic consumption, the steady state dissolved H_2 concentration in the bioreactor is established once the H_2 solubilization and uptake rate becomes equal. In Fig. 6. the H_2 solubilization kinetics by gas injection is compared with slow H_2 uptake kinetics (as in *C. ljungdahlii*) and a fast H_2 uptake kinetics (as in *C. autoethanogenum*) based on the uptake rates obtained from Muñoz et

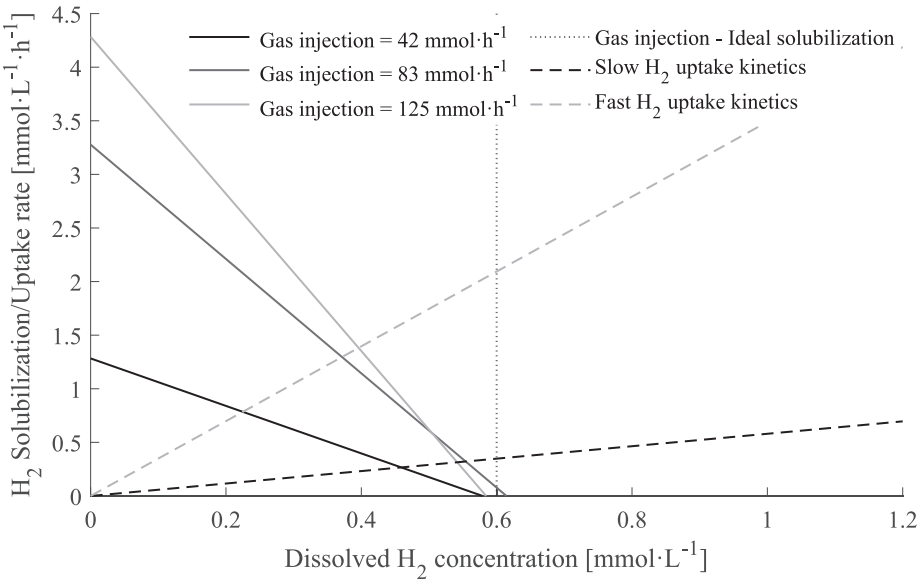

Fig. 6. H_2 Solubilization kinetics of the different H_2 supply rates tested for gas injection (solid lines) and H_2 uptake kinetics (dashed lines) based on the kinetic experiments reported by Muñoz et al [10]. The dotted vertical line represents an ideal gas injection setup where the H_2 gas is instantaneously solubilized (here, 0.6 mmol·L^{-1} was chosen based on the experimental concentration at saturation point).

al at low biomass concentrations (~0.1 g dry weigh·L^{-1}) [10]. Although the first-order kinetics of hydrogenotrophs were only evaluated up to the saturation concentration, here it was extrapolated past this value to elucidate any possible effects on working with supersaturated concentrations.

The higher H_2 supply rates in gas injection allowed decrease the slope of the solubilization kinetics but pivoted close to the saturation concentration. By using the highest injection rate of H_2 gas tested in this work (125 mmol·h^{-1}), it would be possible to maintain a bioreactor working with slow H_2 uptake kinetics at an uptake rate of 0.32 mmol·L^{-1}·h^{-1} with a steady concentration of dissolved H_2 of 0.55 mmol·L^{-1}. For a bioreactor working with fast H_2 uptake kinetics, the maximum uptake rate and dissolved H_2 concentration would be 1.37 mmol·L^{-1}·h^{-1} at 0.39 mmol·L^{-1}. In a system where the H_2 gas injected would instantaneously dissolve but still limited by the saturation concentration (ideal gas sparger, represented by the vertical dotted line), the maximum H_2 uptake rates that could be achieved in the bioreactor for both cases would be 0.35 mmol·L^{-1}·h^{-1} and 2.09 mmol·L^{-1}·h^{-1} respectively. In bioreactors where gas is injected with bubbles larger than a few micrometers, the H_2 uptake rate and concentration of dissolved H_2 would be always limited by the saturation concentration.

Similarly, both H_2 solubilization and biotic uptake kinetics for the case of water electroreduction are shown in Fig. 7.

In water electroreduction, the kinetics of solubilization are not pivoted around the saturation concentration, which allows to have different steady states for the H_2 uptake rate and dissolved concentrations. This is observed on how the solubilization kinetics translate without a pivoted point at different H_2 supply rates. By using the highest rate of H_2 production tested in this work (1.87 mmol·h^{-1}), it would be possible to maintain a bioreactor working with slow H_2 uptake kinetics at an uptake rate of 0.43 mmol·L^{-1}·h^{-1} with a steady concentration of dissolved H_2 of 0.74 mmol·L^{-1}. For a bioreactor working high H_2 uptake

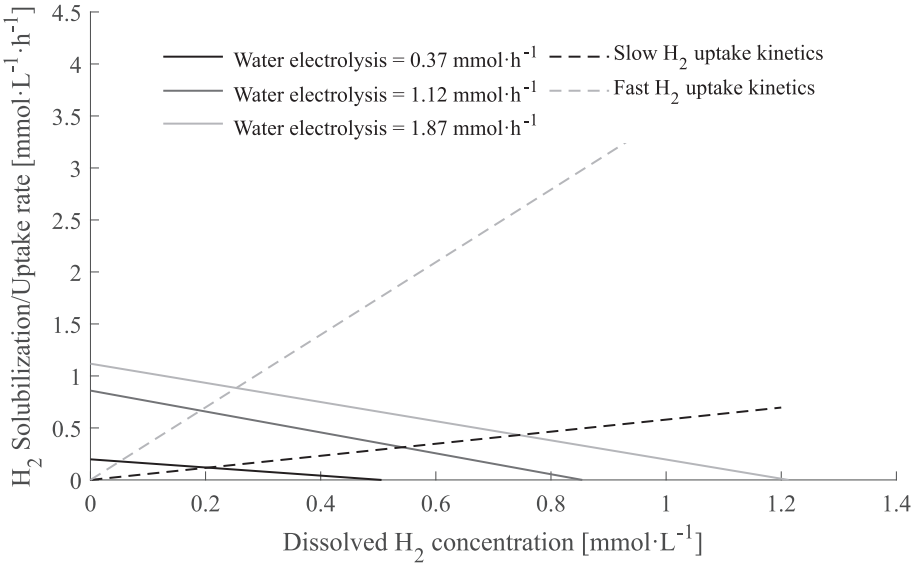

Fig. 7. H_2 Solubilization kinetics of the different H_2 supply rates tested for water electroreduction (solid lines) and H_2 uptake kinetics (dashed lines) based on the kinetic experiments reported by Muñoz et al [10].

kinetics, the steady state H_2 uptake rate and dissolved H_2 concentration would be 0.87 mmol·L^{-1}·h^{-1} at 0.25 mmol·L^{-1}. Even if compared with an ideal gas sparger with instantaneous H_2 solubilization, the water electroreduction technique would be easily more advantageous for bioreactors working with microorganisms characterized by a low H_2 uptake rate. As different H_2 solubilization kinetics result in different dissolved H_2 concentrations, it can be expected that some hydrogenotrophic reactions become more thermodynamically favorable than others. Assuming −20 kJ/mol as the minimum free energy change required for ATP synthesis by chemiosmosis (through translocation of 1 mol of H^+ across the cytoplasmic membrane [44]) and solving Eq. (11) at standard conditions (adjusted for pH = 7), acetogens would require a minimum concentration of dissolved H_2 of ~400 nmol·L^{-1} to overcome this thermodynamic limit, while for methanogens it would be ~11 nmol·L^{-1}. This means that when concentrations fall between these two values, methanogens would outcompete acetogens due to a thermodynamic limitation on the growth of acetogens.

The actual concentration of the species involved in the hydrogenotrophic reactions such as H_2 and CO_2 depends on the balance between the substrate uptake and supply in the bioreactor. In this work, two scenarios with (1) slow H_2 solubilization and (2) fast H_2 solubilization kinetics relative to the H_2 uptake kinetics were evaluated in terms of the thermodynamic potential of a hydrogenotrophic reaction. The results of the modeling of these scenarios are shown in Table 5.

The lowest $k_L^{H_2}a$ to k_1^xX evaluated, with a ratio of 1×10^{-4} resulted in a steady state concentration of C_{H_2} = 78 nmol·L^{-1} and C_{CO_2} = 34.4 mmol·L^{-1} (0.98 bar) at the conditions of gas injection ($C_{H_2}^{sat}$ = 0.78 mM). In this case, only −3.39 kJ·reaction^{-1} would result from the acetogenic reaction, insufficient to overcome the $\Delta G_r = -20$ kJ/reaction needed for growth and outcompete methanogens and sulfate reducers, which would have more favorable thermodynamic potentials of −40 kJ/reaction and − 60 kJ/reaction respectively if calculated. In fact, sulfate reducers and methanogens would have always a $\Delta G_r < -20$ kJ/reaction at the conditions evaluated in this work. In other words, acetogens would be able to outcompete others hydrogenotrophs due to their larger specific growth rates, only when they are not thermodynamically limited [8]. When increasing $k_L^{H_2}a$ to k_1^xX ratio to 1×10^{-3} and beyond, the free energy available quickly becomes larger than the thermodynamic threshold while the characteristic $C_{H_2}^{sat}$ has a less important effect. This means that the best strategy here to favor the thermodynamic potential of acetogenesis is to increase $k_L^{H_2}a$, while working at elevated $C_{H_2}^{sat}$ concentrations (e.g., by bioreactor pressurization or supersaturation by water electroreduction) would have a less important effect in reaching the minimum thermodynamic threshold. It is worth noting that the C_{CO_2} values obtained at steady state in the simulation were close to the saturation concentration, which highlights the higher relevance of controlling the H_2 concentration over the CO_2 concentration. The C_{CO_2} at steady state varied between 88 and 98 % of its saturation concentration, while the C_{H_2} at steady state varied between 0.1 and 10 % of its saturation concentration.

Table 5
Effect of $k_L^{H_2}a$ to k_1^xX ratios and the H_2 saturation concentration ($C_{H_2}^{sat}$) on the Gibbs free energy (ΔG_r) of the acetogenesis and ethanol production reactions (see Table 2).

Scenario 1	ΔG_r (acetogenesis) [kJ·reaction^{-1}]		
$k_L^{H_2}a/k_1^xX$	$C_{H_2}^{sat}$ = 0.78 mmol·L^{-1}	$C_{H_2}^{sat}$ = 3.12 mmol·L^{-1}	$C_{H_2}^{sat}$ = 5.46 mmol·L^{-1}
0.0001	−3.39	−16.87	−22.14
0.001	−26.22	−39.70	−44.96
0.01	−48.96	−62.44	−67.71
0.1	−70.95	−84.45	−89.75
Scenario 2	ΔG_r (ethanol production) [kJ·reaction^{-1}]		
$k_L^{H_2}a/k_1^xX$	$C_{H_2}^{sat}$ = 0.78 mmol·L^{-1}	$C_{H_2}^{sat}$ = 3.12 mmol·L^{-1}	$C_{H_2}^{sat}$ = 5.46 mmol·L^{-1}
1	−17.48	−24.36	−27.13
10	−20.45	−27.32	−30.10
100	−20.87	−27.74	−30.52
1000	−20.92	−27.79	−30.56

The CO_2 and H_2 concentrations at steady state were obtained from the solution of Eqs. (9) and (10) for an acetogenic reaction, while the rest of species were maintained at standard conditions.

For the second scenario, higher $k_L^{H_2}a$ to k_1^xX ratios were used to obtain the steady state concentrations of H_2 and CO_2. As the acetogenic reaction becomes always thermodynamically feasible (with $\Delta G_r < -70$ kJ/reaction), it is more interesting to calculate the conditions at which ethanol production would become feasible.

As opposed to the scenario 1, the best strategy would be to work at supersaturation levels where the characteristic $C_{H_2}^{sat}$ is greater than 0.78 mmol·L^{-1}. For example, if working at a total pressure of 1 bar, the lowest ΔG_r value that could be obtained with a $k_L^{H_2}a$ to k_1^xX ratio greater than 10 seems to reach a minimum of −21 kJ/reaction. This is because at a ratio of 10, the dissolved H_2 concentration is already at the 90 % of the saturation value (0.78 mM) and higher ratios only logarithmically approach to 100 % of the saturation value. Nevertheless, if water electroreduction is used, a value of $\Delta G_r = -24$ kJ/reaction could be obtained with only a $k_L^{H_2}a$ to k_1^xX ratio of 10 and $C_{H_2}^{sat} = 3.12$ mmol·L^{-1}. This is consistent with what is shown in Fig. 6. and Fig. 7, where for a low H_2 uptake rate relative to the solubilization rate (large $k_L^{H_2}a$ to k_1^xX ratio), even an instantaneous solubilization by gas injection with $C_{H_2}^{sat} = 0.78$ mmol·L^{-1} would maintain a lower growth rate than a system where supersaturation ($C_{H_2}^{sat} > 0.78$ mmol·L^{-1}) is achieved. Therefore, for hydrogenotrophic reactions where the H2 concentration seems to be more important such as in the production of ethanol, achieving a higher concentration of H_2 by raising the characteristic $C_{H_2}^{sat}$ (e.g., by pressurization or supersaturation) is the best approach to consider.

4. Discussion

4.1. *Increasing the H_2 solubilization rate while maintaining high solubilization efficiency*

Overcoming H_2 solubilization limitations should be the first step when working with bioreactors involving hydrogenotrophs. In both gas injection and water electroreduction, larger solubilization rates were achieved by increasing the H_2 supply rate. Nevertheless, for H_2 gas injection, the H_2 supply rate did not linearly increase the H_2 solubilization rate. At increasing H_2 supply rates, we can expect that the interfacial area (the 'a' in K_La) also increases as long as bubbles do not coalesce. At the highest H_2 supply rate used here, it is hypothesized that a higher bubble coalescence was occurring during the injection (which also reduces the bubble residence time and consequently, the H_2 solubilization rate). While small pores produce bubbles with small diameters, they are also more prone to bubble coalescence. Therefore, although there is a proportionality of $K_La \propto d_b^{-1}$ where d_b is the bubble diameter, this proportionality can drop to $K_La \propto d_p^{-0.1}$ when considering the pore diameter d_p of spargers in bubble columns [14]. When using gas sparger, the pore size and distribution must be carefully selected to avoid excessive bubble coalescence at high H_2 supply rates. In bubble columns and stirred tank reactors operating at high gas flowrates, bubble coalescence becomes rather unavoidable, and achieving proper bubble breakup and dispersion (e.g., by impeller design, mechanical energy input or induced turbulence) plays a more important role on achieving high k_La values [14].

In water electroreduction, other challenges arise when working at high currents. The first challenge to overcome is due to the high internal resistance of the cell which translates into high energy costs. Optimal reactor designs with low internal resistance (with low interelectrode gap) should be used to avoid large cell voltages. The H-type cell

configuration, although useful for studying electrode reactions, is impractical for electrolysis scale-up. The large cell voltage (around 7 V for 100 mA) in our experiments was mainly attributed to the internal resistance of the H-type cell, while the overpotential associated with the HER reaction alone was less than 2 V (data not shown), limiting the maximum current that could be applied. The second challenge at high currents comes with maintaining local and homogeneously distributed low current densities to avoid bubble nucleation. Similar to how bubble coalescence reduces the solubilization efficiency during gas injection, large current densities facilitate bubble nucleation during water electroreduction, also reducing the solubilization efficiency and therefore the solubilization rate.

To avoid bubble nucleation, electrode designs with large surface areas should be used instead. The use of large cathodic surface areas helps to avoid large local supersaturation of dissolved H_2 in the cathode surface, which is the first requirement for bubble nucleation. In this sense, while high dissolved H_2 concentrations are desired in the bulk phase and not in the localities of the cathode surface, the cathode design and the hydrodynamic flow in the cathodic chamber should also be optimized to allow the easy removal of dissolved H_2 out of the cathode surface into the bulk phase. In this regard, some strategies should be explored such as improved passive transport (by capillary effect) or by active transport by mechanical convection (by agitation), and flow-through porous electrodes.

Passive transport utilizing the capillary effect, particularly through the use of hydrophobic porous membranes such as expanded polytetrafluoroethylene (ePTFE) like Gore-Tex membranes, has been recently proposed as a promising strategy to remove dissolved H_2 out of the cathode surface in a configuration called "bubble-free" electrolysis [45]. Electrodes incorporating PTFE-based Gortex gas diffusion layers coated with catalysts have demonstrated besides achieving low cell onset potentials, the elimination of bubble nucleation, at least to the naked eye. The operational principle relies on the aerophilic nature of the PTFE material, which exhibits a strong affinity for gases. It is suggested that as soon as H_2 gas is produced at the cathodic surface, by its hydrophobic nature, it preferentially adsorbs and transports the H_2 molecules through the PTFE surface away the catalyst layers due to its strong capillary force [46].

Instead of a passive transport by capillary force, an active transport of dissolved H_2 out of the cathode surface can be used during water electrolysis at high currents. Instead of applying a mixing force to agitate the whole bulk liquid around the cathode surface as in H-type cells, the fluid can also be forced through the porosity or the 3D geometry of the cathode in what is commonly known as flow cells. Although flow cells are less used in laboratory setups compared to H-type cells, their higher area to volume ratios and enhanced mass transfer could be more suited for preventing the accumulation of dissolved H_2 near the cathode surface [47]. The enhanced mass transfer is primarily driven by an efficient convective transport, which supplements the slower process of molecular diffusion.

4.2. The dissolved H_2 concentration as a selective variable for controlling competition among hydrogenotrophs and product selection

Different concentrations of dissolved H_2 may favor certain hydrogenotrophic microorganisms over others depending on the energetic gain and metabolic pathways used at each concentration of dissolved H_2. Comparing hydrogenotrophic microorganisms by the Gibbs free energy change of the catabolic reaction, sulfate reducers should have an energetic advantage for growth ($\Delta G^{0'} = -152.2$ kJ/mol from sulfate to sulfide), followed by methanogens ($\Delta G^{0'} = -131$ kJ/mol from CO_2 to methane) and finally acetogens ($\Delta G^{0'} = -95$ kJ/mol from CO_2 to acetate) [48].

However, the Gibbs free energy of the catabolic reaction alone is insufficient to determine the energetic gain or ATP gain for each microorganism and accurately predict competitive advantages. Muñoz et al found experimentally that hydrogenotrophs performing the same acetogenic reaction have different H_2 thresholds spanning from 44 nmol·L^{-1} to 15,000 nmol·L^{-1} and which are proportional to ATP gains [7]. They also found that while ATP gains were genus-specific, H_2 uptake rates were strain-specific, suggesting that growth kinetic differences could originate from enzymes involved in the energy conservation mechanisms coupled with the Wood–Ljungdahl pathway [10].

In bioreactors limited by a slow H_2 solubilization rate, low concentrations of dissolved H_2 dictate the competition among hydrogenotrophs, where only microorganisms with lower H_2 thresholds thrive. In a bioreactor with a H_2 solubilization rate large enough to maintain dissolved H_2 concentrations above common H_2 thresholds, hydrogenotrophic microorganisms using metabolic pathways with high specific H_2 uptake rates may outcompete the ones using metabolic pathways with low specific H_2 uptake rates. For single strains capable of switching metabolic pathways according to the substrate concentration, high concentrations of dissolved H_2 might favor the use of metabolic pathways with high H_2 uptake rates even if they allow lower ATP gains as described by the resource allocation theory [49].

The shift on metabolic strategies and fluxes in acetogens are dictated by the thermodynamics of these metabolic fluxes, more than the common gene-regulation found in other microorganisms [50]. The thermodynamic potential of each metabolic flux depends on the balance of its involved redox pairs ($NADPH/NADP^+$, $NADG/NAD^+$, Fd_{red}/Fd_{ox}) and the concentration of intermediate metabolites (e.g., acetate) [50]. As the H_2 is involved in the balance of these redox pools, different dissolved H_2 concentrations should also affect the flux of these metabolic pathways and therefore the product selectivity. In *C. autoethanogenum*, the shift from acetate to ethanol formation at high dissolved H_2 concentrations occurs when sufficient H_2 supply leads to high biomass and undissociated acetic acid concentrations in a bioreactor. The resulting intracellular acetate accumulation disrupts ATP homeostasis, and ethanol production via the aldehyde:ferredoxin oxidoreductase (AOR) pathway helps restore balance [51,52]. In mixed cultures, chain elongation likely occurs by the coupling of the Wood-Ljungdahl pathway where acetate and ethanol is generated first and then cyclically elongated to medium-chain carboxylic acids by the fatty acid biosynthesis (FAB) pathway and the reverse β-oxidation pathway, where maintaining high concentrations of dissolved H_2 (or reducing equivalents) avoids the oxidation of the elongated carboxylic acids [53–55]. Similarly, excessive ethanol oxidation (EEO, present in some hydrogenotrophs) is a competing metabolic pathway against alcohol production where the most common approach to suppress EEO is to work at high concentrations of dissolved H_2 to maintain the EEO reaction thermodynamically unfeasible [56].

High concentrations of dissolved H_2 also influence the competitive dynamics between Rnf- and Ech- acetogens. These organisms use the Rnf or Ech membrane-bound enzymatic complex to couple electron transport with ion translocation across the membrane, a process which is ultimately responsible for ATP synthesis. In Rnf-acetogens, the end product of respiration is NADH, which can be redirected into other NADH-reducing metabolic pathways. In contrast, Ech-acetogens produce H_2 as a respiration product [4]. As a result, high concentrations of dissolved H_2 can create a thermodynamic backpressure, potentially inhibiting Ech-acetogens over Rnf-acetogens. Furthermore, high concentrations of dissolved H_2 can also cause direct metabolic inhibition. For instance, in *A. woodie*, biomass growth and acetate production declined when the H_2 partial pressure of the inlet gas increased from 0.4 bar to 1.4 bar and 2.1 bar. This decline was accompanied by an accumulation of formate (a key precursor in the Wood-Ljungdahl pathway) [57]. Similarly, in a genetically engineered strain of *M. thermoacetica* designed for ethanol production, high concentrations of H_2 inhibited its growth, which was not observed in the wild-type strain. This inhibition was linked to the disruption of the NAD^+/NADH redox balance, which could be mitigated by the introduction of an external electron acceptor [58].

These findings highlight the importance of controlling the dissolved H_2 concentration in hydrogenotrophic processes. Maintaining an optimal concentration of H_2 is essential not only for regulating microbial growth and interspecies competition, but also for maximizing product yields. Moreover, operating across a wider range of dissolved H_2 concentrations could expand the spectrum of viable metabolic fluxes in hydrogenotrophic systems.

4.3. Achieving high concentrations of dissolved H_2 is technically challenging

Operating at high concentrations of dissolved H_2 is industrially relevant for achieving high growth and production rates, and for potentially shifting metabolic pathways towards long-chain metabolites. However, achieving such high concentrations presents significant technical challenges. In this work, the maximum concentration of dissolved H_2 achieved by gas injection, regardless of the H_2 supply rate, consistently remained below 0.78 mM, which is the H_2 saturation concentration at 1 bar and 25C.

Higher hydrostatic pressures in tall columns or operating with pressurized reactors increase the H_2 saturation concentration, in accordance with Henry's law. Demler et al. observed that the cell-specific productivities for hydrogenotrophic acetate production by *A. woodii* increased linearly with increasing H_2 partial pressures (0.4–1.7 bar, corresponding to 0.3–1.3 mmol·L^{-1} of dissolved H_2) in the reactor headspace [59]. Stoll et al. similarly reported increased cell and product concentrations when increasing the total pressure from 1 to 4 bar in a syngas-fed reactor (H_2/CO/CO_2/N_2: 48/16/16/20). However, a negative effect was observed at 7 bar, which they attributed to the pressurization rate not being sufficiency slow to allow for cell adaptation [60]. For comparison, a partial H_2 pressure of 1.55 bar would be required for gas injection to match the 1.21 mmol H_2·L^{-1} achieved by water electroreduction at 1 bar of total pressure. Achieving this H_2 partial pressure by gas injection would require a total reactor pressure of 2 bar in a reactor using a gas mixture of high purity at H_2: CO2 of 3:1; or 7.75 bar with a gas mixture containing 20 % H_2. Alternatively, the internal bubble pressure can also be increased by producing bubbles of smaller sizes (micro/nanobubbles), owing to the Laplace pressure. It can be roughly estimated that H_2 bubbles of 30 μm of diameter would have to be injected to reach a dissolved H_2 concentration of just 15 % above the H_2 saturation concentration at 25C in water, according to the Epstein-Plesset solution for the dissolution of H_2 bubbles [18]. However, the practical size of generated bubbles is restricted by sparger fouling; in industrial settings, coarse gas spargers typically produce bubbles with diameters larger than 1 mm [61].

A more effective approach for injecting H_2 microbubbles into the liquid medium can be also achieved by water electroreduction. In this case, high current densities are used to initiate bubble nucleation, yielding significantly smaller bubbles compared to those produced by traditional gas spargers. Gao et al. managed to produce microbubbles with diameters below 150 μm using a CoP-NiF electrode, maintaining a dissolved H_2 concentration of 0.63 mmol·L^{-1} in the presence of hydrogenotrophic methanogens [62]. Cui et al. generated bubbles ranging from 25 to 750 μm using an inexpensive stainless steel felt band as an electrode, achieving a H_2 supersaturation concentration of 1 mmol·L^{-1} and proving its applicability within a MES producing acetate [16]. Commercial devices capable of producing micro/nanobubbles from gas injection are also available. For example, Moleaer nanobubble injector (www.moleaer.com) can produce nanobubbles with a mean bubble diameter of ~120 nm. Micro/nanobubble production and stability represent a growing research field, although its applicability to processes involving hydrogenotrophs requires further validation.

When using water electroreduction to produce dissolved H_2, the maximum concentration of dissolved H_2 achievable in the bulk liquid is ultimately limited by the local concentration at which the dissolved H_2 nucleates on the cathodic surface. In this study, a maximum concentration of 1.21 mmol·L^{-1} was achieved at the highest electrochemical H_2 supply rate. The concentration at the bulk liquid is expected to be lower than the local concentration at the cathode surface (the upper limit). The proximity of the dissolved H_2 concentration in the bulk liquid to this upper limit depends on the rate at which the dissolved H_2 is transported away from the cathode surface. Using Eq. (3) from the classical nucleation theory, it can be estimated that a local supersaturation approximately 1450-fold is required initiate bubble nucleation, assuming a zero contact angle at the nucleation site (as in homogeneous nucleation) [26,41]. Nevertheless, this value does not account for surface heterogeneities on the cathode that could alter the contact angle at the nucleation site. For platinum nanoelectrodes of varying sizes (radii = 7–41 nm), a local supersaturation of approximately 300-fold was found to be necessary for the start of H_2 bubble nucleation. This corresponds to a dissolved H_2 concentration of 0.23 mol·L^{-1} on the cathode surface with a contact angle of 150°, a value specific to the extent of surface heterogeneities and cathode's hydrophilicity [63]. In this study, although the local critical concentration for nucleation was not estimated, it is safe to assume that the maximum dissolved H_2 concentrations achievable in the bulk liquid were not limited by the local supersaturation concentration. This observation arises from the linear relationship obtained between the H_2 supply rate (imposed current) and the maximum dissolved H_2 concentration, suggesting that even higher concentrations in the bulk liquid could be potentially achieved as long as proper mixing is ensured. This linear relationship was also observed by others in a continuous water electroreduction cell, where the effect of working at high electrolyte flow rates (improved mixing) eclipsed the negative effects of the electrode roughness on achieving high dissolved H_2 concentrations [64].

It is worth noting that using the electrolyte supersaturated in H_2 as a growth medium for hydrogenotrophic bioprocesses can bring additional challenges. The reduction of water in the cathodic chamber can increase the pH of the medium if the pH is not adequately controlled. Moreover, the solid biomass and inorganic particles can act as potential nucleation sites when the solution is supersaturated with H_2. Other soluble compounds with surfactant activity (e.g., dissolved CO2, extracellular proteins) that could be inevitably present in the cathodic chamber may also facilitate the nucleation of bubbles at the cathode surface. Future research on the extent of degassing should be further tested in a hydrogenotrophic spent medium.

4.4. Solubilization and energy efficiency

Different strategies must be implemented to improve the solubilization efficiency according to the solubilization technique used. For gas injection, improving energy efficiency is linked to enhancing the solubilization efficiency. Gas recirculation is employed to prolong the bubble residence time within the liquid medium, thereby increasing solubilization. However, this solubilization efficiency can decrease if the population of bubbles become too large, potentially promoting coalescence. Larger coalesced bubbles have larger volumes and thus higher rise velocities, paradoxically leading to a decrease in the overall residence time and consequently affecting solubilization efficiency [14].

For water electroreduction, the first step to improve the energy efficiency should come from the use of cell designs with low internal resistance and cell voltage. Reducing the cell voltage by using a cell with low interelectrode gap as in parallel flow through cells, could significantly improve energy efficiency. Similarly, it would be convenient to work with electrolytes with high ionic conductivity to reduce the internal resistance of the cell. Although this is usually achieved by increasing the salinity of the electrolyte, high concentrations of ions such as Na^+ can disfavor the growth of non-halophilic microorganisms [65].

The choice of cathode material is also fundamental to achieve with lower cell voltages. While noble metals such as platinum and rhodium exhibit the highest electrocatalytic activity for HER [66], their high cost

renders their use economically unfeasible in applications with low-value products such as in hydrogenotrophic processes. Transition metals such as nickel and iron have high electrocatalytic activity for HER, but at a significantly reduced cost. Nickel alloys (e.g., Ni—Mo, Ni—Fe) are most commonly used due to their high electrocatalytic activity and corrosion resistance. Finally, carbon-based materials are also employed due to their high surface area and corrosion resistance, although they are typically doped with heteroatoms or combined with transition metals to enhance their electrocatalytic activity [67].

The next step towards improving energy efficiency during water electroreduction involves minimizing the formation of H_2 bubbles at the cathode surface. This can be achieved by using cathode materials with optimized structures, such as porous and 3D electrodes, that prevent H_2 accumulation at their surface. Moreover, cell designs such as the use of thin electrodes in flow through cells should be investigated on their current distribution homogeneity. The efficient use of the cathode surface by homogeneous current distributions should also bring a reduction in the local maximum current density and therefore (by avoiding bubble formation) a better solubilization/energy efficiency.

The inherent advantage in energy efficiency obtained by water electroreduction for dissolved H_2 production stems from the fact that the H_2 produced does not necessarily form a separate gas phase before dissolving. This is reflected in an 18-fold higher solubilization efficiency compared to gas injection. If the water electroreduction cell were designed to produce gaseous H_2 for subsequent injection and solubilization in a separate step, water electroreduction would require approximately 1.8 times more energy than if it was produced via SMR.

5. Conclusion

The findings of this study demonstrate that water electroreduction offers a clear advantage over traditional H_2 gas injection for providing dissolved H_2 in bioprocesses. This superiority is evidenced by several key metrics. Notably, water electroreduction achieved a H_2 solubilization efficiency of 35 %, an 18-fold improvement compared to the 2 % efficiency observed with gas injection. This high efficiency allowed for the generation of a supersaturated H_2 concentration of 1.21 $mmol \cdot L^{-1}$, whereas gas injection was limited to a maximum dissolved H_2 concentration of 0.62 $mmol \cdot L^{-1}$ (close to saturation concentration of 0.78 $mmol \cdot L^{-1}$). Furthermore, even with an H_2 production rate approximately 18 times lower than that of gas injection, water electroreduction achieved a comparable H_2 solubilization rate of 0.67 $mmol \cdot L^{-1} \cdot h^{-1}$, aligning closely with the 0.79 $mmol \cdot L^{-1} \cdot h^{-1}$ rate obtained via gas injection. These results underscore the potential of water electroreduction as an effective method for providing the high H_2 concentrations required to optimize processes involving hydrogenotrophs, where supersaturation can significantly influence product selectivity and microbial competition.

CRediT authorship contribution statement

Juan-Diego Carvajalino-Olave: Writing – original draft, Visualization, Software, Methodology, Investigation, Formal analysis, Data curation, Conceptualization. **Léa Laguillaumie:** Writing – review & editing, Conceptualization. **Claire Dumas:** Writing – review & editing, Visualization, Supervision, Resources, Project administration, Methodology, Funding acquisition, Conceptualization. **Benjamin Erable:** Writing – review & editing, Visualization, Supervision, Resources, Project administration, Methodology, Funding acquisition, Conceptualization.

Declaration of Generative AI and AI-assisted technologies in the writing process

During the preparation of this work the author(s) used Gemini 2.5 Flash in order to improve readability and language. After using this tool/service, the author(s) reviewed and edited the content as needed and take(s) full responsibility for the content of the published article.

Declaration of competing interest

The authors declare the following financial interests/personal relationships which may be considered as potential competing interests: Juan Diego Carvajalino Olave reports financial support was provided by Carnot 3BCar Institute. If there are other authors, they declare that they have no known competing financial interests or personal relationships that could have appeared to influence the work reported in this paper.

Acknowledgments

The authors gratefully acknowledge the provided financial support by the Carnot Institute 3BCAR through the HYSSYH project and the BioEco Graduate School.

Appendix A. Supplementary data

Supplementary data to this article can be found online at https://doi.org/10.1016/j.cej.2025.168494.

Data availability

Data will be made available on request.

References

[1] R.K. Thauer, K. Jungermann, K. Decker, Energy conservation in chemotrophic anaerobic bacteria, Bacteriol. Rev. 41 (1) (Mar. 1977) 100–180, https://doi.org/10.1128/br.41.1.100-180.1977.
[2] R.K. Thauer, The Wolfe cycle comes full circle, Proc. Natl. Acad. Sci. 109 (38) (Sep. 2012) 15084–15085, https://doi.org/10.1073/pnas.1213193109.
[3] H.L. Drake, in: Harold Drake (Ed.), Acetogens, 1994.
[4] A. Katsyv, V. Müller, Overcoming energetic barriers in acetogenic C1 conversion, Front. Bioeng. Biotechnol. 8 (December) (2020) 1–23, https://doi.org/10.3389/fbioe.2020.621166.
[5] P. Dessì, et al., Microbial electrosynthesis: towards sustainable biorefineries for production of green chemicals from CO2 emissions, Biotechnol. Adv. 46 (July 2020) (2021), https://doi.org/10.1016/j.biotechadv.2020.107675.
[6] P. Albina, N. Durban, A. Bertron, A. Albrecht, J.-C. Robinet, B. Erable, Influence of hydrogen electron donor, alkaline pH, and high nitrate concentrations on microbial denitrification: a review, Int. J. Mol. Sci. 20 (20) (2019) 5163, https://doi.org/10.3390/ijms20205163.
[7] M. Laura, P. Jo, No acetogen is equal: strongly different H $_2$ thresholds reflect diverse bioenergetics in acetogenic bacteria, Environ. Microbiol. 25 (10) (Oct. 2023) 2032–2040, https://doi.org/10.1111/1462-2920.16429.
[8] L. Laguillaumie, et al., Controlling the microbial competition between hydrogenotrophic methanogens and homoacetogens using mass transfer and thermodynamic constraints, J. Clean. Prod. 414 (Aug. 2023) 137549, https://doi.org/10.1016/j.jclepro.2023.137549.
[9] O.R. Kotsyurbenko, M.V. Glagolev, A.N. Nozhevnikova, R. Conrad, Competition between homoacetogenic bacteria and methanogenic archaea for hydrogen at low temperature, FEMS Microbiol. Ecol. 38 (2–3) (Dec. 2001) 153–159, https://doi.org/10.1111/j.1574-6941.2001.tb00893.x.
[10] L. Muñoz-Duarte, S. Chakraborty, L.V. Grøn, M.F. Bambace, J. Catalano, J. Philips, H_2 consumption by various acetogenic bacteria follows first-order kinetics up to H_2 saturation, Biotechnol. Bioeng. 122 (4) (Apr. 2025) 804–816, https://doi.org/10.1002/bit.28904.
[11] IEA (2024), "Global Hydrogen Review 2024," IEA, Paris, 2024. [Online]. Available: https://www.iea.org/reports/global-hydrogen-review-2024.
[12] F. Liew, M.E. Martin, R.C. Tappel, B.D. Heijstra, C. Mihalcea, M. Köpke, Gas fermentation—a flexible platform for commercial scale production of low-carbon-fuels and chemicals from waste and renewable feedstocks, Front. Microbiol. 7 (May 2016), https://doi.org/10.3389/fmicb.2016.00694.
[13] V. Linek, M. Kordač, T. Moucha, Mechanism of mass transfer from bubbles in dispersions, Chem. Eng. Process. Process Intensif. 44 (1) (Jan. 2005) 121–130, https://doi.org/10.1016/j.cep.2004.05.009.
[14] E. Kadic, T.J. Heindel, An Introduction to Bioreactor Hydrodynamics and Gas-Liquid Mass Transfer, 1st ed., Wiley, 2014 https://doi.org/10.1002/9781118869703.
[15] W. Chuenchart, R. Karki, T. Shitanaka, K.R. Marcelino, H. Lu, S.K. Khanal, Nanobubble technology in anaerobic digestion: a review, Bioresour. Technol. 329 (Jun. 2021) 124916, https://doi.org/10.1016/j.biortech.2021.124916.
[16] K. Cui, K. Guo, J.M. Carvajal-Arroyo, J. Arends, K. Rabaey, An electrolytic bubble column with an external hollow fiber membrane gas–liquid contactor for effective

microbial electrosynthesis of acetate from CO2, Chem. Eng. J. 471 (Sep. 2023) 144296, https://doi.org/10.1016/j.cej.2023.144296.
[17] R. H. Perry and D. W. Green, Eds., Perry's chemical engineers' handbook, 7. ed., [3. Nachdr.]. In Perry's Chemical Engineers' Platinum Edition. New York, NY: McGraw-Hill, 1999.
[18] P.S. Epstein, M.S. Plesset, On the stability of gas bubbles in liquid-gas solutions, J. Chem. Phys. 18 (11) (Nov. 1950) 1505–1509, https://doi.org/10.1063/1.1747520.
[19] D.R. Lovley, Electromicrobiology, Annu. Rev. Microbiol. 66 (2012) 391–409, https://doi.org/10.1146/annurev-micro-092611-150104.
[20] E. Marsili, X. Zhang, Shuttling via soluble compounds, in: K. Rabaey, L. Angenent, P. Lens, U. Schroder, J. Keller (Eds.), Bioelectrochemical Systems: From Extracellular Electron Transfer to Biotechnological Application, IWAP Publishing, UK, 2009.
[21] P.L. Tremblay, L.T. Angenent, T. Zhang, Extracellular electron uptake: among autotrophs and mediated by surfaces, Trends Biotechnol. 35 (4) (2017) 360–371, https://doi.org/10.1016/j.tibtech.2016.10.004.
[22] R. Karthikeyan, R. Singh, A. Bose, Microbial electron uptake in microbial electrosynthesis: a mini-review, J. Ind. Microbiol. Biotechnol. 46 (9–10) (Oct. 2019) 1419–1426, https://doi.org/10.1007/s10295-019-02166-6.
[23] I. Vassilev, P. Dessì, S. Puig, M. Kokko, Cathodic biofilms – a prerequisite for microbial electrosynthesis, Bioresour. Technol. 348 (Mar. 2022) 126788, https://doi.org/10.1016/j.biortech.2022.126788.
[24] Z. Liu, X. Xue, W. Cai, K. Cui, S.A. Patil, K. Guo, Recent progress on microbial electrosynthesis reactor designs and strategies to enhance the reactor performance, Biochem. Eng. J. 190 (Jan. 2023) 108745, https://doi.org/10.1016/j.bej.2022.108745.
[25] H. Lee, J. Bae, S. Jin, S. Kang, B.K. Cho, Engineering acetogenic bacteria for efficient one-carbon utilization, Front. Microbiol. 13 (May) (2022), https://doi.org/10.3389/fmicb.2022.865168.
[26] S.D. Lubetkin, Why is it much easier to nucleate gas bubbles than theory predicts? Langmuir 19 (7) (Apr. 2003) 2575–2587, https://doi.org/10.1021/la0266381.
[27] C. Jin, Y.-L. Liu, Y. Shan, Q.-J. Chen, Scanning electrochemical cell microscope study of individual H2 gas bubble nucleation on platinum: effect of surfactants, Chin. J. Anal. Chem. 49 (4) (Apr. 2021) e21055–e21064, https://doi.org/10.1016/S1872-2040(21)60096-8.
[28] M. Suvira, B. Zhang, Effect of surfactant on electrochemically generated surface nanobubbles, Anal. Chem. 93 (12) (Mar. 2021) 5170–5176, https://doi.org/10.1021/acs.analchem.0c05067.
[29] R. Iwata, et al., Bubble growth and departure modes on wettable/non-wettable porous foams in alkaline water splitting, Joule 5 (4) (Apr. 2021) 887–900, https://doi.org/10.1016/j.joule.2021.02.015.
[30] F. Kracke, et al., Efficient hydrogen delivery for microbial electrosynthesis via 3D-printed cathodes, Front. Microbiol. 12 (Aug. 2021) 696473, https://doi.org/10.3389/fmicb.2021.696473.
[31] E.V. Labelle, C.W. Marshall, H.D. May, Microbiome for the Electrosynthesis of chemicals from carbon dioxide, Acc. Chem. Res. 53 (1) (2020) 62–71, https://doi.org/10.1021/acs.accounts.9b00522.
[32] E. Blanchet, F. Duquenne, Y. Rafrafi, L. Etcheverry, B. Erable, A. Bergel, Importance of the hydrogen route in up-scaling electrosynthesis for microbial CO2 reduction, Energ. Environ. Sci. 8 (12) (Dec. 2015) 3731–3744, https://doi.org/10.1039/c5ee03088a.
[33] X. Lu, et al., Hydrogen bubble evolution and gas transport mechanism on a microelectrode determined by cathodic potential and temperature, Phys. Fluids 36 (7) (Jul. 2024) 073302, https://doi.org/10.1063/5.0213398.
[34] P.A. Kempler, R.H. Coridan, L. Luo, Gas evolution in water electrolysis, Chem. Rev. 124 (19) (Oct. 2024) 10964–11007, https://doi.org/10.1021/acs.chemrev.4c00211.
[35] B.T. Sangtam, H. Park, Review on bubble dynamics in proton exchange membrane water electrolysis: towards optimal green hydrogen yield, Micromachines 14 (12) (Dec. 2023) 2234, https://doi.org/10.3390/mi14122234.
[36] A.J. Bard, L.R. Faulkner, Electrochemical Methods: Fundamentals and Applications, 2nd ed., Wiley, New York, 2001.
[37] E.V. LaBelle, H.D. May, Energy efficiency and productivity enhancement of microbial electrosynthesis of acetate, Front. Microbiol. 8 (May 2017) 756, https://doi.org/10.3389/fmicb.2017.00756.
[38] P.L. Spath, M.K. Mann, Life cycle assessment of hydrogen production via natural gas steam reforming, NREL/TP-570-27637 764485 (Sep. 2000), https://doi.org/10.2172/764485.
[39] M. Schalenbach, G. Tjarks, M. Carmo, W. Lueke, M. Mueller, D. Stolten, Acidic or alkaline? Towards a new perspective on the efficiency of water electrolysis, J. Electrochem. Soc. 163 (11) (2016) F3197–F3208, https://doi.org/10.1149/2.0271611jes.
[40] F. Ale Enriquez, B.K. Ahring, Strategies to overcome mass transfer limitations of hydrogen during anaerobic gaseous fermentations: a comprehensive review, Bioresour. Technol. 377 (Jun. 2023) 128948, https://doi.org/10.1016/j.biortech.2023.128948.
[41] S. Lubetkin, The motion of electrolytic gas bubbles near electrodes, Electrochim. Acta 48 (4) (Dec. 2002) 357–375, https://doi.org/10.1016/S0013-4686(02)00682-5.
[42] K. Kikuchi, et al., Hydrogen particles and supersaturation in alkaline water from an alkali–ion–water electrolyzer, J. Electroanal. Chem. 506 (1) (Jun. 2001) 22–27, https://doi.org/10.1016/S0022-0728(01)00517-4.
[43] K. Kikuchi, Y. Tanaka, Y. Saihara, M. Maeda, M. Kawamura, Z. Ogumi, Concentration of hydrogen nanobubbles in electrolyzed water, J. Colloid Interface Sci. 298 (2) (Jun. 2006) 914–919, https://doi.org/10.1016/j.jcis.2006.01.010.
[44] H.L. Drake, Acetogenesis, Chapman & Hall, 1994.
[45] P. Tiwari, G. Tsekouras, K. Wagner, G.F. Swiegers, G.G. Wallace, A new class of bubble-free water electrolyzer that is intrinsically highly efficient, Int. J. Hydrogen Energy 44 (42) (Sep. 2019) 23568–23579, https://doi.org/10.1016/j.ijhydene.2019.07.100.
[46] G.F. Swiegers, R.N.L. Terrett, G. Tsekouras, T. Tsuzuki, R.J. Pace, R. Stranger, The prospects of developing a highly energy-efficient water electrolyser by eliminating or mitigating bubble effects, Sustain. Energy Fuels 5 (5) (2021) 1280–1310, https://doi.org/10.1039/D0SE01886D.
[47] D. Pletcher, R.A. Green, R.C.D. Brown, Flow electrolysis cells for the synthetic organic chemistry laboratory, Chem. Rev. 118 (9) (May 2018) 4573–4591, https://doi.org/10.1021/acs.chemrev.7b00360.
[48] M.A. Lever, Acetogenesis in the energy-starved deep biosphere – a paradox? Front. Microbiol. 2 (2012) https://doi.org/10.3389/fmicb.2011.00284.
[49] A. Regueira, J.M. Lema, M. Mauricio-Iglesias, Microbial inefficient substrate use through the perspective of resource allocation models, Curr. Opin. Biotechnol. 67 (Feb. 2021) 130–140, https://doi.org/10.1016/j.copbio.2021.01.015.
[50] M. Pavan, et al., Advances in systems metabolic engineering of autotrophic carbon oxide-fixing biocatalysts towards a circular economy, Metab. Eng. 71 (May 2022) 117–141, https://doi.org/10.1016/j.ymben.2022.01.015.
[51] K. Valgepea, et al., Maintenance of ATP homeostasis triggers metabolic shifts in gas-fermenting acetogens, Cell Syst. 4 (5) (May 2017) 505–515.e5, https://doi.org/10.1016/j.cels.2017.04.008.
[52] H. Richter, B. Molitor, H. Wei, W. Chen, L. Aristilde, L.T. Angenent, Ethanol production in syngas-fermenting Clostridium ljungdahlii is controlled by thermodynamics rather than by enzyme expression, Energ. Environ. Sci. 9 (7) (2016) 2392–2399, https://doi.org/10.1039/C6EE01108J.
[53] M.T. Agler, C.M. Spirito, J.G. Usack, J.J. Werner, L.T. Angenent, Development of a highly specific and productive process for n-caproic acid production: applying lessons from methanogenic microbiomes, Water Sci. Technol. 69 (1) (Jan. 2014) 62–68, https://doi.org/10.2166/wst.2013.549.
[54] J. De Jesús Montoya-Rosales, P. Núñez-Valenzuela, A. Ontiveros-Valencia, M. Morales-Ibarría, S. Revah, E. Razo-Flores, From syngas fermentation to chain elongation: the role of key microorganisms and multi-omics analysis, Bioenergy Res. 17 (2) (Nov. 2023) 897–911, https://doi.org/10.1007/s12155-023-10696-2.
[55] C.M. Spirito, H. Richter, K. Rabaey, A.J. Stams, L.T. Angenent, Chain elongation in anaerobic reactor microbiomes to recover resources from waste, Curr. Opin. Biotechnol. 27 (Jun. 2014) 115–122, https://doi.org/10.1016/j.copbio.2014.01.003.
[56] C. Quintela, et al., Excessive ethanol oxidation versus efficient chain elongation processes, Waste Biomass Valoriz. 15 (4) (Apr. 2024) 2545–2558, https://doi.org/10.1007/s12649-023-02323-0.
[57] C. Kantzow, D. Weuster-Botz, Effects of hydrogen partial pressure on autotrophic growth and product formation of Acetobacterium woodii, Bioprocess Biosyst. Eng. 39 (8) (Aug. 2016) 1325–1330, https://doi.org/10.1007/s00449-016-1600-2.
[58] S. Kobayashi, et al., Reversible hydrogenase activity confers flexibility to balance intracellular redox in Moorella thermoacetica, Front. Microbiol. 13 (May 2022) 897066, https://doi.org/10.3389/fmicb.2022.897066.
[59] M. Demler, D. Weuster-Botz, Reaction engineering analysis of hydrogenotrophic production of acetic acid by *Acetobacterium woodii*, Biotechnol. Bioeng. 108 (2) (Feb. 2011) 470–474, https://doi.org/10.1002/bit.22935.
[60] I.K. Stoll, N. Boukis, J. Sauer, Syngas fermentation at elevated pressure - experimental results, Proc. 27th Eur. Biomass Conf. Exhib. 27–30 May 2019 (2019) 7, https://doi.org/10.5071/27THEUBCE2019-3CV.3.4.
[61] P.M. Wilkinson, A.P. Spek, L.L. Van Dierendonck, Design parameters estimation for scale-up of high-pressure bubble columns, AICHE J. 38 (4) (Apr. 1992) 544–554, https://doi.org/10.1002/aic.690380408.
[62] J.-Y. Gao, et al., Strengthening H2 gas–liquid mass transfer using superaerophobic cathodes for enhanced methane production from CO2 in H2-mediated microbial electrosynthesis system, Bioresour. Technol. 417 (Feb. 2025) 131850, https://doi.org/10.1016/j.biortech.2024.131850.
[63] S.R. German, M.A. Edwards, H. Ren, H.S. White, Critical nuclei size, rate, and activation energy of H_2 gas nucleation, J. Am. Chem. Soc. 140 (11) (Mar. 2018) 4047–4053, https://doi.org/10.1021/jacs.7b13457.
[64] Y. Tanaka, K. Kikuchi, Dissolution of hydrogen produced by water electrolysis: effects of electrode roughness factor and current density, Results Chem. 5 (Jan. 2023) 100984, https://doi.org/10.1016/j.rechem.2023.100984.
[65] P. Dessì, et al., Microbial electrosynthesis of acetate from CO2 in three-chamber cells with gas diffusion biocathode under moderate saline conditions, Environ. Sci. Ecotechnol. 16 (Oct. 2023) 100261, https://doi.org/10.1016/j.ese.2023.100261.
[66] A.R. Zeradjanin, J. Grote, G. Polymeros, K.J.J. Mayrhofer, A critical review on hydrogen evolution electrocatalysis: re-exploring the volcano-relationship, Electroanalysis 28 (10) (Oct. 2016) 2256–2269, https://doi.org/10.1002/elan.201600270.
[67] W. Zhou, et al., Recent developments of carbon-based electrocatalysts for hydrogen evolution reaction, Nano Energy 28 (Oct. 2016) 29–43, https://doi.org/10.1016/j.nanoen.2016.08.027.
[68] J.J. Reed, The NBS Tables of Chemical Thermodynamic Properties: Selected Values for Inorganic and C1 and C2 Organic Substances in SI Units, in: National Institute of Standards and Technology, 2020, https://doi.org/10.18434/M32124.
[69] W. Cai, et al., An electrolytic-hydrogen-fed moving bed biofilm reactor for efficient microbial electrosynthesis of methane from CO2, Chem. Eng. J. 428 (Jan. 2022) 132093, https://doi.org/10.1016/j.cej.2021.132093.
[70] K. Valgepea, et al., H2 drives metabolic rearrangements in gas-fermenting Clostridium autoethanogenum, Biotechnol. Biofuels 11 (1) (Dec. 2018) 55, https://doi.org/10.1186/s13068-018-1052-9.